

Available online at www.sciencedirect.com

ScienceDirect

journal homepage: www.elsevier.com/locate/he

Effects of heat exchanger design on the performance of a solid state hydrogen storage device

Anurag Singh^a, M.P. Maiya^{a,*}, S.Srinivasa Murthy^b

^a Refrigeration and Air Conditioning Laboratory, Department of Mechanical Engineering, Indian Institute of Technology Madras, Chennai 600036, India

^b Interdisciplinary Center for Energy Research (ICER), Indian Institute of Science, Bangalore 560012, India

ARTICLE INFO

Article history:

Received 7 April 2015

Received in revised form

1 June 2015

Accepted 4 June 2015

Available online 30 June 2015

Keywords:

Heat exchanger

Metal hydride

Hydrogen storage

Heat and mass transfer

Copper fins

ABSTRACT

Heat exchanger design plays a significant role in the performance of solid state hydrogen storage device. In the present study, a cylindrical hydrogen storage device with an embedded annular heat exchanger tube with radial circular copper fins, is considered. **A 3-D mathematical model of the storage device is developed** to investigate the sorption performance of metal hydride (MH). **A prototype of the device is fabricated for 1 kg of MH alloy, LaNi₅, and tested at constant supply pressure of hydrogen, validating the simulation results.** Absorption characteristics of storage device have been examined by varying different operating parameters such as **hydrogen supply pressure and cooling fluid temperature** and velocity. **Absorption process is completed in 18 min when these parameters are 15 bar, 298 K and 1 m/s respectively.** A study of geometric parameters of copper fins (such as perforation, number and thickness of fin) has been carried out to investigate their effects on absorption process.

Copyright © 2015, Hydrogen Energy Publications, LLC. Published by Elsevier Ltd. All rights reserved.

Introduction

Disadvantages and inadequacies of conventional non-renewable energy sources have involved researchers from all around the world to find an alternative. Hydrogen has been considered as a promising candidate, but its poor energy density by volume (0.0898 g/L) has made its storage a major bottleneck towards the hydrogen economy. Conventional methods to store hydrogen in its physical form such as high pressure gas storage and liquefaction (cryogenic storage) are very unsafe and energy intensive. Solid state storage of

hydrogen in metal hydride (chemical storage) is gaining importance due to several advantages such as compactness and safety due to normal temperature and pressure operations. The storage device must be designed to absorb sufficient amount of hydrogen within a short interval of time. Absorption/desorption process of hydrogen is associated with considerable heat release/uptake, but poor thermal conductivity of MH decelerates the process and increases the charging/discharging time. Previous studies clarify that an effective heat management system for the storage device can significantly increase the absorption/desorption rate to reduce the charging/discharging time. Various inner and outer heat

* Corresponding author.

E-mail address: mpmaiya@iitm.ac.in (M.P. Maiya).

<http://dx.doi.org/10.1016/j.ijhydene.2015.06.015>

0360-3199/Copyright © 2015, Hydrogen Energy Publications, LLC. Published by Elsevier Ltd. All rights reserved.

exchanger designs have been investigated theoretically and experimentally in the literature and the former has generated a lot of interest amongst the researchers.

Combined heat and mass transfer phenomenon controls the charging time of metal hydride. Ben Nasrallah et al. [1] tested the validity of the assumptions made to simplify the heat and mass transfer analysis of the hydrogen storage device by comparing the numerical results with and without the assumptions for LaNi_5 . They concluded that the local thermal equilibrium between solid and gas is valid under almost all conditions. The effect of pressure variation in the storage device and convection heat transport term can be neglected. The effect of concentration variation can be seen only during desorption process, whereas it can be neglected during the absorption process. Ram Gopal and Srinivasa Murthy [2,3] experimentally investigated the performance of a cylindrical hydrogen storage device for different heat transfer fluid temperatures. Mohan et al. [4] simulated the performance of LaNi_5 based hydrogen storage device with embedded filters and heat exchanger tubes. They found bed thickness to be a major parameter controlling the sorption reaction. Mellouli et al. [5] conducted experiments on a storage device equipped with a spiral heat exchanger tube and concluded that the heat exchanger which provides more heat transfer area reduces the charging time significantly. Muthukumar et al. [6] studied the heat and mass transfer process in a 2-D model of an annular cylindrical hydrogen storage device. Mellouli et al. [7] presented a 2-D mathematical model of a storage device and investigated the effect of adding metal foam with the MH material. They found that aluminum foam increases the heat transfer rate and hence reduces the charging time by 60% for 90% storage of hydrogen. Askri et al. [8] examined the storage device incorporating a concentric heat exchanger tube with fins and a good improvement in the performance was found. Mellouli et al. [9] compared the effects of spiral tube heat exchanger with and without fins on charging time and 66% improvement for 90% hydrogen storage is reported for the former design. Anbarasu et al. [10] experimentally investigated the absorption performance of $\text{LaNi}_{4.91}\text{Sn}_{0.15}$ based solid state hydrogen storage device with 36 and 60 embedded cooling tubes. They investigated the effects of different operating parameters on absorption rate and absorption capacity. The reduction in absorption time for storage device with 60 tubes was quite significant (37.5%) as compared to 36 cooling tubes. Souahlia et al. [11] conducted the experimental studies on two different designs of storage device, first one with finned concentric heat exchanger tube embedded inside the MH bed and the second one with conventional concentric heat exchanger jacket, using LaNi_5 as a storage media. A good absorption rate was found for first design. Mandhapati and Kumar [12] presented a systematic study to optimize the heat exchanger design using CFD modeling for three different shell and tube heat exchanger configurations. They concluded that a helical coil heat exchanger is useful to get a high heat transfer coefficient because of high turbulence and consequently the enhanced absorption rate. Linder et al. [13] experimentally investigated the effects of main influencing parameters on the dynamics of a MH reaction bed using $\text{LaNi}_{4.91}\text{Sn}_{0.15}$ as a hydriding material. They used capillary tube bundle heat exchanger and a very fast charging time of

about 100 s was obtained for 1 g of MH at water flow rate of 5 l/min. Anbarasu et al. [14] presented the simulation analysis of a cylindrical MH storage device with embedded cooling tubes. They first simulated the 2-D model to optimize the number of embedded cooling tubes. The study was then further extended to develop a 3-D model to predict the sorption performance of $\text{LaNi}_{4.91}\text{Sn}_{0.15}$ under different operation conditions of supply pressure, hot fluid temperature and effective thermal conductivity. Several other heat exchanger mechanisms such as helical coil heat exchanger with Al foam [15], heat pipe [16], embedded cooling tubes [17], finned multi-tubular tank [18] and finned spiral heat exchanger and lateral heat exchanger [19] for storage devices were investigated in the recent past. The effects of different operating variables such as hydrogen supply pressure, heat transfer fluid temperature and overall heat transfer coefficient were studied by many researchers [2,4,5,7,8,11,12,17–19] and it was concluded that a good choice of these parameters is necessary to improve the sorption performance. Mazzucco et al. [20] reviewed the recent works on heat management systems of hydrogen storage device focusing on the limitations and performance improvement of each system.

All the above studies indicate a strong dependence of charging/discharging time of MH storage device on its heat exchanger design. However, a proper numerical study of heat and mass transfer process in a solid state hydrogen storage device with experimental validation and investigation of effects of different heat exchanger configurations is limited. The objectives of this work is to study experimentally and theoretically the hydrogen absorption process in a solid state hydrogen storage device with an embedded heat exchanger of novel design. The effects of different geometric parameters of the fins and various operating conditions on absorption performance were investigated vis-à-vis reduced charging time.

Experimental analysis

Description of hydrogen storage device

The proposed design of MH hydrogen storage device is shown in Fig. 1. It is a cylindrical device with embedded finned heat exchanger assembly. The cross sectional view of storage device at different sections are shown in Fig. 1(a). The dimensions of the storage device are given in Table 1. According to the capacity of device, 1 kg of MH, LaNi_5 , is filled inside the cylinder. A circular opening on the cylinder serves as an inlet/outlet port for hydrogen gas. Unit cell of packed MH bed is shown in Fig. 1(b). Heat exchanger design employs two concentric stainless steel tubes with copper fins as shown in Fig. 2(a). Water is used as a heat transfer fluid which enters into the heat exchanger through the inner tube from top of the storage device, and is redirected through a concentric annular outer tube from bottom to top. In order to increase the heat transfer between the fluid and MH bed, thirteen radial circular copper fins are equally spaced on the periphery of outlet tube. Design of the circular copper fin is presented in Fig. 2(b). Holes are punched in the fin to reduce the total weight of the heat exchanger assembly. Three PT-100 sensors are inserted inside the device, each to a different depth of 50, 90 and 130 mm from

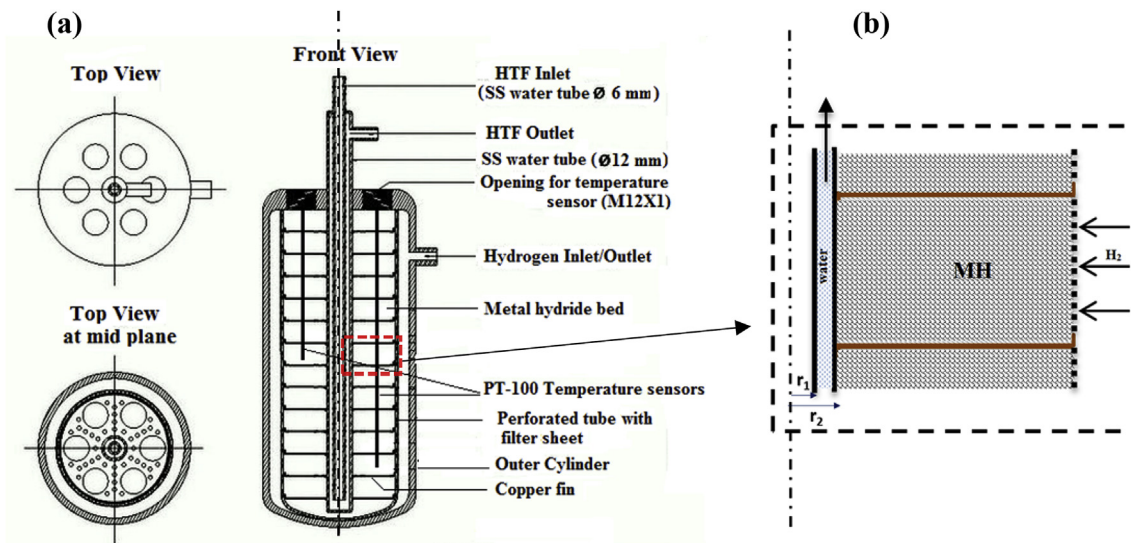


Fig. 1 – Proposed metal hydride hydrogen storage device (a) Cross sectional view at different sections; (b) Unit cell of packed metal hydride bed.

Table 1 – Dimensions of the hydrogen storage device

Sl. No.	Geometrical Parameters	Value
1.	Height (mm)	140
2.	Diameter (mm)	72
3.	Inner coolant tube diameter (mm)	6
4.	Outer coolant tube diameter (mm)	12
5.	Fin diameter (mm)	52
6.	Fin thickness (mm)	0.5
7.	Fin spacing (mm)	9.5
8.	Top flange thickness (mm)	10

the top flange through each larger hole. The positions of the sensors are shown in Fig. 1(a). MH lumps are inserted to the storage device through the remaining three larger holes.

Experimental method

A prototype of the storage device described in Section 2.1 is fabricated and tested for model validation. The experimental setup is constructed with three main circuits, namely, gas line

circuit (open), heat transfer fluid circuit and electrical circuit. Gas line circuit is constructed with $\frac{1}{4}$ inch seamless stainless steel (SS316) tube and high pressure packless type bellow valves. Two piezo resistive type pressure transducers, a rotary vacuum pump, hydrogen and argon cylinders with valves, a coriolis type mass flow meter and a hydrogen filter are connected in the gas line circuit. In the heat transfer fluid circuit, a thermostatic bath (temperature range of -20 to 300 °C) with an integrated pump is used to circulate fluid at constant temperature during the experiments. In the electrical circuit the temperature sensors PT-100 and thermocouples are directly connected to the data acquisition system, whereas the mass flow meter and pressure transducers are connected through a DC source to the data acquisition system for logging data to a computer. MH alloy is activated inside the storage device by repetitive cycles of absorption and desorption at certain supply/desorption pressures of hydrogen and fluid temperatures. Experiments are performed once MH is activated. Metal hydride is allowed to absorb hydrogen gas at constant supply pressure and constant temperature of heat

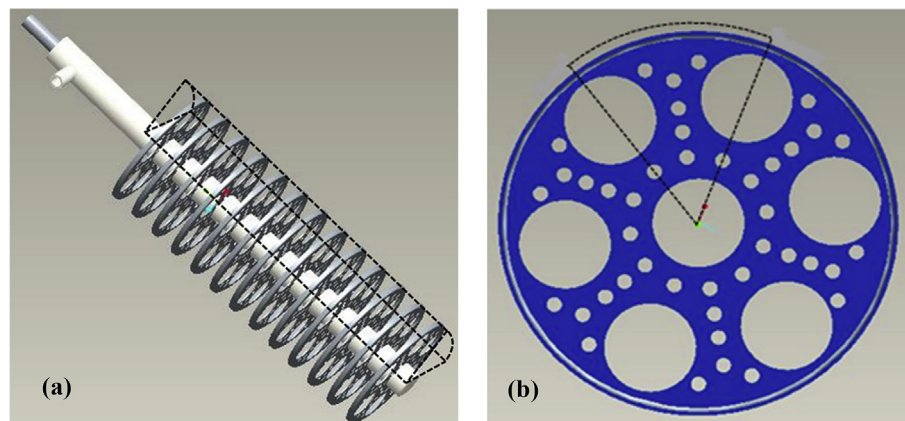


Fig. 2 – Pictorial view of (a) Heat exchanger assembly and (b) Copper fin used in the storage device.

transfer fluid. Performance parameters such as mass flow rate, MH bed temperature, gas pressure and heat transfer fluid temperature are recorded continuously in the computer from data logger. The rate and amount of hydrogen absorbed is obtained directly from the mass flow meter. The average bed concentration during the absorption process is estimated from the obtained rate data. Hence, the storage capacity of the device is calculated as:

$$\text{Storage capacity (wt\%)} = \frac{\text{Mass of hydrogen absorbed (g)}}{\text{Mass of alloy used (g)}} \times 100 \quad (2.1)$$

Mathematical model

Problem formulation

Sorption performance of LaNi₅ based hydrogen storage device under different operating conditions is simulated using commercial FEA package COMSOL Multiphysics. Model used for analysis is drawn using model builder wizard, integrated with COMSOL Multiphysics. Due to the symmetry of the storage device, 1/6th part is modeled to reduce the computational time. The dotted portion in Fig. 2(a) and (b) show the 1/6th part of the heat exchanger assembly and copper fin respectively, used in the simulation geometry. Mass balance and energy balance differential equations in MH bed with specified initial and boundary conditions are imposed in the model used for the analysis. Due to large number of variables and complications in the numerical simulation, the following assumptions are made to simplify the problem:

1. Local thermal equilibrium exists between solid and gas within the bed.
2. Porous hydride bed is homogeneous and isotropic.
3. Thermophysical properties of the metal hydride bed such as thermal conductivity and permeability are independent of temperature, pressure and concentration.
4. Convection heat transfer within the bed is neglected, since velocity of hydrogen gas is very small. Only the conduction heat transfer is considered.
5. Hydrogen behaves as a perfect gas, since the pressure within the bed is moderate.

Governing equations and boundary conditions

Due to absorption/desorption of hydrogen and the corresponding evolution of heat, transient variations exist within the hydride bed. Based on the above assumptions, the following equations are used for simulation of the storage device.

Volume averaged energy balance equation

Volume averaged energy balance equation for the hydride bed is expressed as:

$$(\rho c_p)_e \frac{\partial T}{\partial t} = \nabla \cdot (k_e \nabla T) - (1 - \varepsilon) \dot{m} \Delta H \quad (3.1)$$

Where, $(\rho c_p)_e$ is the effective volumetric heat capacity and k_e is the effective thermal conductivity which are given by:

$$(\rho c_p)_e = \varepsilon (\rho c_p)_g + (1 - \varepsilon) (\rho c_p)_{mh} \quad (3.2)$$

$$k_e = \varepsilon k_g + (1 - \varepsilon) k_{mh} \quad (3.3)$$

An additional heat source term $[(1 - \varepsilon) \dot{m} \Delta H]$ is added in the right hand side of Eq. (3.1), which represents the total heat generated during the absorption/desorption process. Here ΔH denotes the heat of formation for MH. Energy balance equation for copper fins, heat exchanger tube walls and top flange cover can be expressed as Eq. (3.1), by removing the heat source term in the right hand side.

Volume averaged mass balance equation

The volume averaged mass balance equation for MH and hydrogen can be expressed as follows:

$$(1 - \varepsilon) \frac{\partial \rho}{\partial t} = \dot{m} + (1 - \varepsilon) \nabla \cdot (-D \nabla \rho) \quad (3.4)$$

The L.H.S. of the Eq. (3.4) is the change of (volumetric) MH mass with time and the R.H.S. is the generation/absorption rate of hydrogen (also per m³ of MH). Here, D is the diffusivity and expressed as:

$$D = D_0 \exp\left(\frac{-H_a}{k_B T}\right) \quad (3.5)$$

where, H_a is the activation enthalpy and k_B is the Boltzmann constant.

Reaction kinetics

The mass rate of hydrogen absorbed and desorbed per unit volume of metal hydride is denoted by \dot{m}_a and \dot{m}_d respectively and can be expressed as [21]:

$$\text{For absorption: } \dot{m}_a = C_a \exp\left(\frac{E_a}{RT}\right) \ln\left(\frac{P}{P_{eq}}\right) (\rho_{sat} - \rho_{mh}) \quad (3.6)$$

$$\text{For desorption: } \dot{m}_d = -C_d \exp\left(\frac{E_d}{RT}\right) \left(\frac{P - P_{eq}}{P_{eq}}\right) (\rho_{mh} - \rho_{alloy}) \quad (3.7)$$

Where, ρ_{sat} represents the density of hydride at saturation and ρ_{alloy} denotes density of MH alloy LaNi₅. P_{eq} denotes the equilibrium pressure inside the storage device during the sorption phenomena and is determined by the van't Hoff relationship [19]:

$$\ln(P_{eq}) = A - \frac{B}{T} + \alpha \times \tan\left(\pi \times \left(\frac{x}{x_0} - \frac{1}{2}\right)\right) + \frac{\beta}{2} \quad (3.8)$$

where, A and B are van't Hoff constants. α and β denote the plateau slope and hysteresis factor respectively. x_0 represents the maximum hydrogen fraction (wt%) for MH alloy.

Governing equation for heat exchanger tube

Fluid flow takes place inside the annular space between inner and outer tube at constant flow rate. Energy balance equation within the fluid is given as:

$$(\rho c_p)_f \frac{\partial T_f}{\partial t} + (\rho c_p)_f \vec{v} \cdot \nabla T_f = \nabla \cdot (k_f \nabla T_f) \quad (3.9)$$

Initial and boundary conditions

Initial conditions. Initially the hydride bed temperature, pressure and density are assumed to be uniform. Therefore,

$$T = T_0; \quad P = P_0; \quad \rho = \rho_0 \quad \text{at } t = 0. \quad (3.10)$$

Boundary conditions. Reaction heat is transferred from/to the MH bed by heat transfer fluid which is circulating inside the tube of heat exchanger assembly. No slip condition is valid at the tube walls. Upper, lower and side walls of storage device are adiabatic. Based on the above conditions, the boundary conditions are written as follows:

At the outside walls:

$$(-k \nabla T) \cdot \vec{n} = 0 \quad (3.11)$$

At the heat exchanger tube wall side:

$$(-k \nabla T) \cdot \vec{n} = h(T_f - T) \quad (3.12)$$

Thermophysical properties of different materials used in the simulation study are given in Table 2 [6,22].

Grid independence test

A grid independence test for the proposed 3-D model is carried out comparing the effects of different grid sizes on computation time during the absorption process. An unstructured mesh is used and different grid sizes increasing from coarse to fine are chosen for the study. The results obtained from numerical simulation are compared in Table 3. It is observed that as the number of elements are increased from 80000 (coarse mesh) to 320886 (fine mesh), the computational time doubles due to increased number of elements. However, the result accuracy does not change when the number of elements are increased from 320886 (Fine mesh) to 520771 (Extra fine). Fine grid size with number of elements 320886 are used to carry out the present simulation.

Model validation

Numerical simulation results are compared with experimental results to validate the mathematical model. The

average bed concentration during the absorption process is measured using mass flow meter and compared with volume averaged concentration obtained from simulation study for two different supply pressures of hydrogen ($P_s = 5$ bar and 15 bar) at cooling fluid temperature of 298 K and flow velocity of 1 m/s in Fig. 3(a). It can be seen that the two plots match quite well. The model slightly overpredicts the experimental results. The reason for the slight deviation is due to the assumptions made during numerical simulation. The average bed temperature is recorded with the help of three PT-100 sensors placed inside the device at different locations (50, 90 and 130 mm from top flange) and validated with the simulation result in Fig. 3(b). Numerical results agree with experimental results both in the trend and value.

Results and discussion

Absorption characteristics

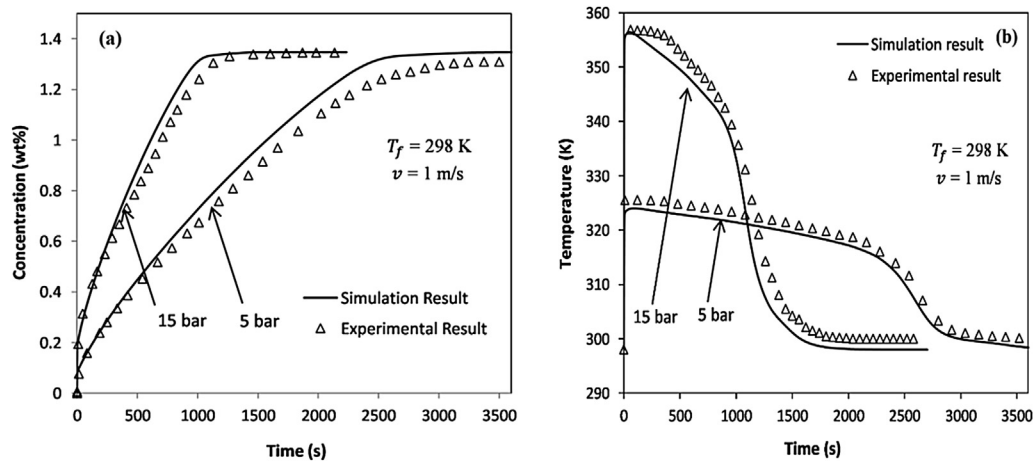
Absorption characteristics of MH hydrogen storage device are investigated at constant supply pressure of 15 bar and cooling fluid temperature of 298 K and velocity of 1 m/s. Fig. 4 depicts the average bed concentration and average bed temperature with respect to charging time. The concentration and temperature curve can be well understood with the help of Fig. 5. It depicts the absorption rate, which can be categorized into two stages, stage A, at the beginning of the process where absorption rate increases rapidly and reaches to a peak of 17 g/min and then decreases abruptly to a value of around 2 g/min, and stage B, where it decreases gradually from 2 g/min to zero value at the end of the absorption process. In stage A, it can be seen that initially (at time = close to zero) absorption rate is very high, because of the high pressure difference between supply pressure (P_s) and equilibrium pressure of hydride bed inside the storage device (P_{eq}), which is known as driving potential for mass transfer. It absorbs 0.2 wt% of hydrogen during first 10 s and simultaneously the average bed temperature goes up to 356 K. It is because of the rapid absorption rate that a tremendous amount of heat is liberated. The poor thermal conductivity of MH restricts the quick transfer of heat to the

Table 2 – Thermophysical properties of materials.

Sl. No	Parameters	LaNi ₅	Hydrogen	Steel	Copper
1.	Density, ρ (kg m ⁻³)	8200	0.0838	7850	8700
2.	Specific heat, c_p (J kg ⁻¹ K ⁻¹)	419	14890	420	385
3.	Thermal conductivity, k (W m ⁻¹ K ⁻¹)	2.4	0.18	19	400
4.	Porosity, ϵ (–)	0.5	–	–	–
5.	Diffusion coefficient, D_0 (m ² s ⁻¹)	–	4.6e-12	–	–
6.	Plateau slope, α (–)	0.038	–	–	–
7.	Hysteresis factor, β (–)	0.137	–	–	–
8.	Initial concentration of MH bed, c_0 (mol m ⁻³)	18981.6	–	–	–
9.	Activation energy – Absorption, E_a (J mol ⁻¹)	21170	–	–	–
10.	Activation energy – Desorption, E_d (J mol ⁻¹)	16450	–	–	–
11.	Material constant used in Eq. (3.6), C_a (s ⁻¹)	59.187	–	–	–
12.	Material constant used in Eq. (3.7), C_d (s ⁻¹)	9.57	–	–	–
13.	van't Hoff constants used in Eq. (3.8), A (–)	12.99	–	–	–
	B (K)	3704.59	–	–	–

Table 3 – Grid size and time elapsed during absorption process.

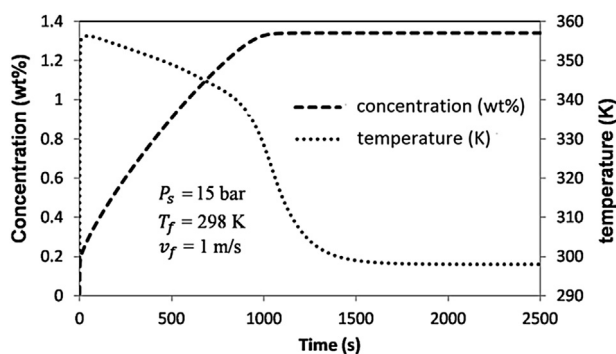
Sl. No.	Grid size/Number of elements	Computational time	Time taken for absorption (12 g of H ₂)
1.	Coarse/80000	1 h 10 min	756 s
2.	Fine/320886	2 h 05 min	802 s
3.	Extra fine/520771	2 h 20 min	806 s

**Fig. 3 – Experimental validation of (a) average bed concentration and (b) average bed temperature during absorption for two different supply pressures.**

cooling fluid and average bed temperature increases. So it is clear that in initial stage A, pressure difference is the major reason for rapid absorption.

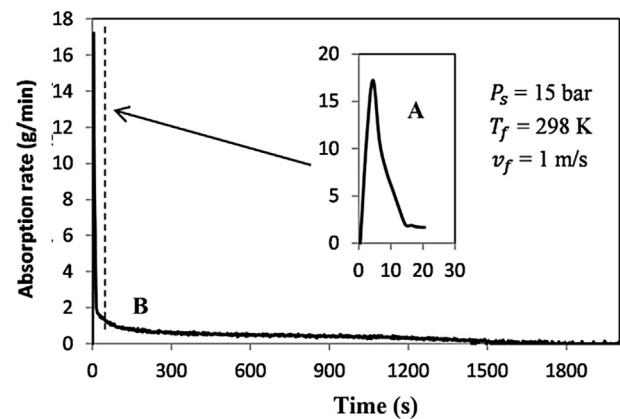
Rapid temperature rise of MH increases the equilibrium pressure inside the device and decreases the driving potential for mass transfer, consequently, the absorption rate decreases abruptly. In stage B, circulating cooling fluid slowly removes the heat from the hydride bed, and thereby continuously reduces the temperature and equilibrium pressure of the hydride bed and further absorption of hydrogen takes place. This process continues till maximum hydrogen is absorbed. It can be understood that in the second stage, heat transfer plays a major role in mass transfer and absorption process. It is found that MH absorbs 1.34 wt% of the hydrogen in 1080 s.

Fig. 6 shows the evolution of MH bed concentration and temperature during absorption process at different time

**Fig. 4 – Absorption characteristics of metal hydride hydrogen storage device.**

intervals of (a) 60 s, (b) 180 s, (c) 420 s and (d) 760 s. It can be observed that the absorption process has two reaction fronts, one propagates from the periphery of cooling tube towards the outer boundary of the MH bed and the other starts from the region near copper fin and propagates towards the adjacent copper fin. The above phenomenon is a consequence of temperature evolution of MH bed, which shows low temperature in the regions near the cooling wall and copper fins. Thus the MH regions near the cooling tube and copper fins are saturated earlier than the other regions.

The variation of heat transfer fluid temperature in the axial direction at different time intervals (60, 180, 540, 900, 1080, and 1200 s) is shown in Fig. 7. The axial distance shown in the x-axis represents the distance from bottom, where heat transfer

**Fig. 5 – Experimental result for absorption rate at constant supply pressure.**

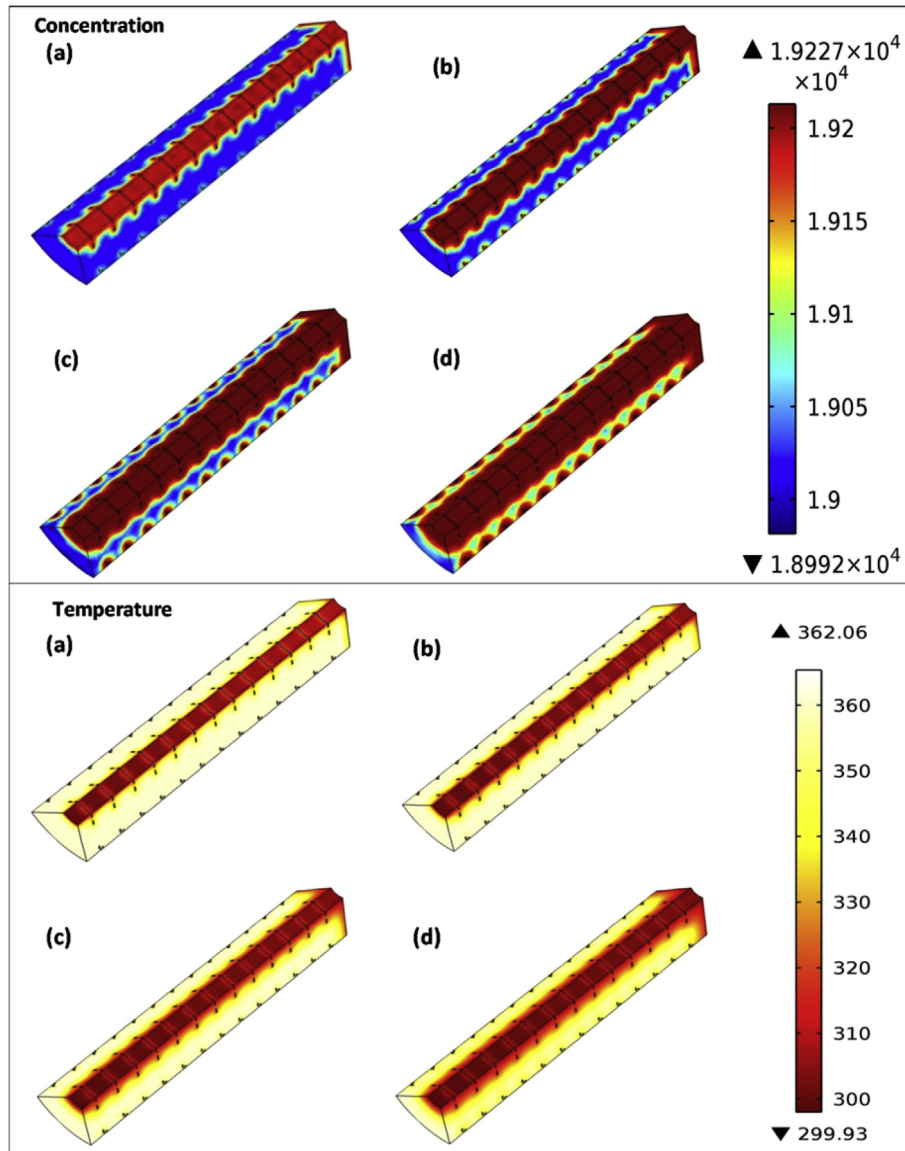


Fig. 6 – Evolution of MH bed concentration and temperature at different time intervals during absorption ($P_s = 15$ bar, $T_f = 298$ K); (a) 60 s, (b) 180 s, (c) 420 s, (d) 760 s.

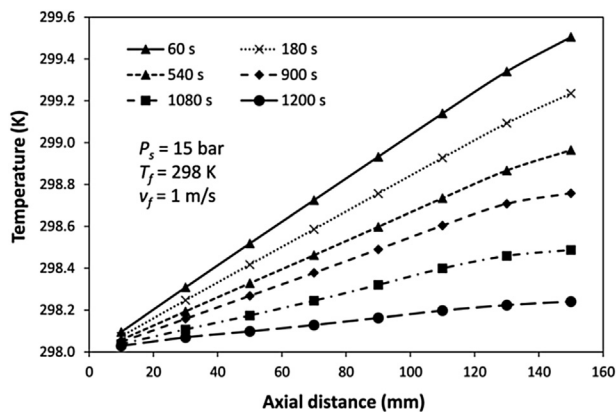


Fig. 7 – Variation of heat transfer fluid temperature in the axial direction at different time intervals.

fluid enters the outer tube of heat exchanger assembly to top where it comes out of the device. It can be seen that the fluid temperature increases in the axial direction from inlet to outlet. Absorption is rapid during initial period. The corresponding large heat release increases the bed temperature rapidly. The heat transfer fluid is to absorb the heat from the MH bed and it can be seen that in the initial period (60 s) the outlet temperature of fluid is maximum i.e. 299.5 K. As the process progresses, absorption becomes less intense and the bed temperature decreases resulting in the fluid temperature to decrease at the outlet. After complete absorption the fluid temperature remains the same as the inlet temperature.

Desorption characteristics

Desorption characteristic of storage device is investigated for a desorption pressure of 1 bar. The heat transfer fluid is

circulated at temperature of 363 K and the initial condition of the MH bed is assumed to have a uniform temperature of 363 K. The concentration and average bed temperature w.r.t. time is presented in Fig. 8. It can be seen that initially because of high equilibrium pressure inside the storage device and high value of mass driving potential, desorption rate is very high. It is found that 0.25 wt% of hydrogen desorbs in the first 20 s and bed temperature reaches to 297 K. The magnified view of concentration vs time plot up to 20 s is also shown in Fig. 8. Desorption rate slows down because of reduction in bed temperature and equilibrium pressure. Later, due to transfer of heat from hot fluid to hydride bed, bed temperature goes up and further desorption takes place at almost constant rate. It is found that it takes only 920 s to desorb 1.3 wt% of hydrogen.

Performance analysis

Heat and mass transfer evolution during absorption process typically depends upon the heat exchanger design of the storage device. The faster it transfers the heat of absorption to the cooling fluid, the faster the hydride bed approaches to saturation. In this section, the effects of different fin configurations on average bed concentration and temperature evolution are investigated. Also, the effects of different operating parameters (such as hydrogen supply pressure and cooling fluid temperature and velocity) are examined. These parameters are varied in a specified range and given in Table 4. Bold letters represent the parameter value around which other parameters are changed.

Effect of number of fins

Fig. 9(a) and (b) depict the effect of number of fins on average bed concentration and temperature. It can be observed that increasing number of fins enhances the heat transfer rate to cooling fluid and thus improves the absorption characteristics of the MH bed. For example, to absorb 1 wt% of hydrogen (i.e. 10 g), configuration with 13 fins takes only 614 s while configuration with 3 fins takes 1400 s. It can be seen from Fig. 5 that in initial stage A, for all configurations, bed temperature reaches to the same peak of around 356 K but in the second stage B, configuration with more number of copper fins shows good heat transfer characteristics and bed temperature quickly approaches to the predefined temperature of cooling fluid. For example, at time $t = 2000$ s, bed temperature is found

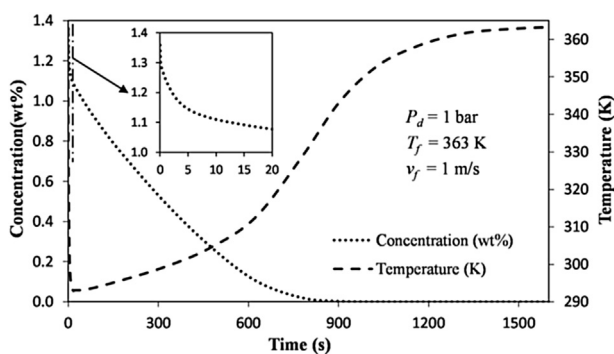


Fig. 8 – Desorption characteristics of hydrogen storage device.

Table 4 – Parameter ranges used in simulation study.

Sl. No.	Parameters	Ranges
1.	Numbers of copper fins	3, 7, 10, 13
2.	Thickness of copper fins (mm)	0.5, 1, 1.5
3.	Hydrogen supply pressure, P_s (bar)	7, 9, 11, 13, 15
4.	Cooling fluid temperature, T_f (K)	288, 293, 298 , 303, 308
5.	Cooling fluid velocity, v (m s ⁻¹)	0.25, 0.5, 0.75, 1

to be 300 K for configuration with 13 fins whereas it is 334 K for configuration with 3 fins. Fig. 9(c) displays the MH bed temperature distribution at different positions along x-y axis at time $t = 1000$ s for (a) 7 fins, (b) 10 fins and (c) 13 fins. It clearly demonstrates that MH bed temperature for configuration with 7 fins is much higher after 1000 s when compared with 13 fins.

Effect of fin thickness

The average bed concentration and temperature for different fin thicknesses are demonstrated in Fig. 10(a) and (b) respectively. Increasing fin thickness enhances the heat transfer kinetics and improves the sorption characteristic of MH bed. However, the improvement is not much significant for 1.5 mm when compared to 1 mm thick copper fin.

Fig. 10(c) depicts the evolution of copper fin temperature at time $t = 120$ s, 720 s and 1000 s for different fin thicknesses (a) 0.5 mm, (b) 1 mm and (c) 1.5 mm. It is clear that 1.5 mm thick copper fin reduces the temperature more efficiently as compared to 0.5 mm thick fin. For instance at time $t = 1000$ s, copper fin temperature is only 300 K in case of 1.5 mm, whereas it is found to be much higher at around 335 K in case of 0.5 mm. Moreover an argument can be made that increasing the number of fins and its thickness will significantly increase the thermal weight of the system and subsequently increase the sensible heating and cooling requirement. Also it will reduce the space for MH powder inside the storage device. Therefore a trade-off between the performance and thermal mass of the fin is required in order to improve the performance.

Effect of fin perforation

The weight of the storage device including heat transfer assembly is an important factor and should be optimized for improved gravimetric capacity. In the present model, 42 holes of 2 mm diameter and 6 holes of 12 mm diameter in circular manner, are punched in copper fin which results in reducing its weight as well as the surface area for heat transfer by 44%. Effects of perforation in copper fin on average bed concentration and temperature are shown in Fig. 11 (a) and (b) respectively. It is clear from the figure that copper fin without perforation improves the heat transfer and thus reduces the time required for complete absorption. The improvement is only 13% for absorption of 1 wt% (10 g of hydrogen) in case of copper fin without perforation at the cost of 44% higher weight.

In the experimental setup, as mentioned earlier, a few large holes are required in the fin to insert both MH lumps and sensor probes for temperature measurement. However to study the effects of different numbers and diameters of holes

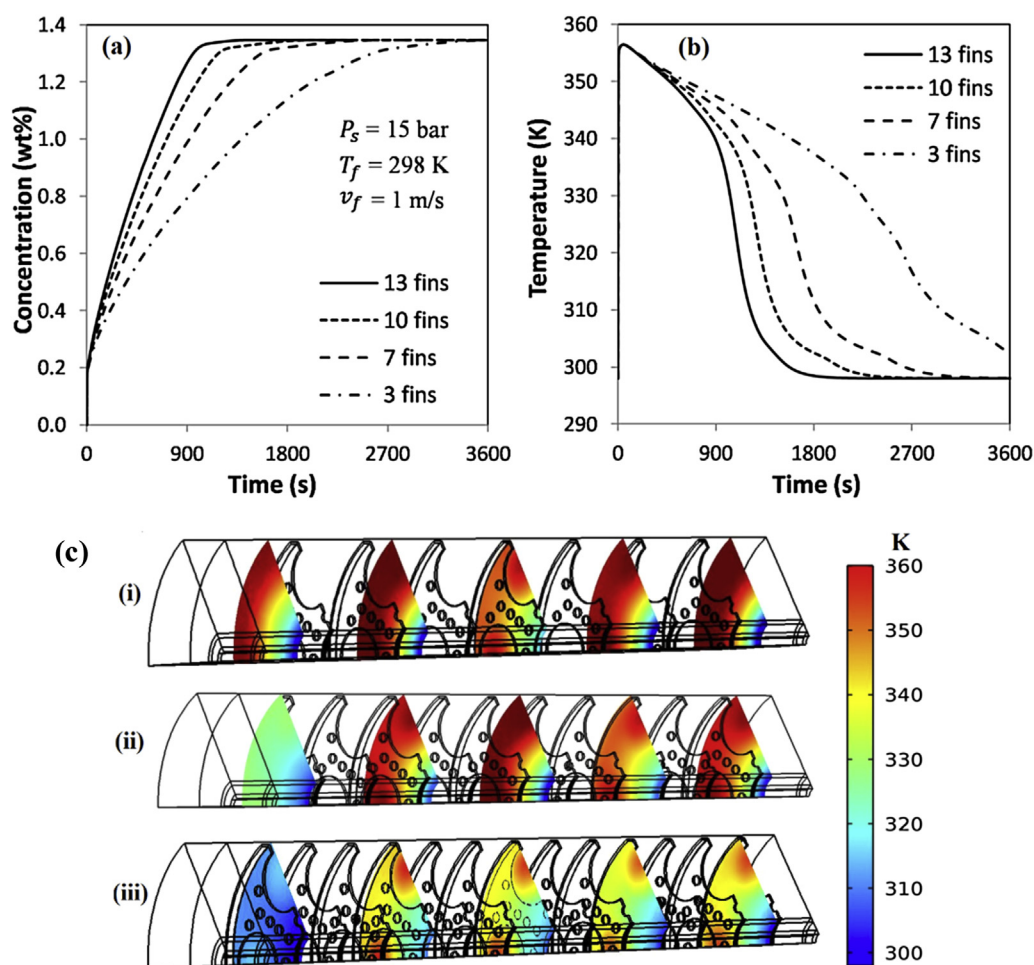


Fig. 9 – Effect of number of fins on (a) average bed concentration; (b) average bed temperature and (c) temperature distribution in MH bed at $t = 1000$ s; (i) 7 fins, (ii) 10 fins, (iii) 13 fins.

on absorption performance, an analysis is carried out keeping the mass of the fin constant at 5.37 g. The surface area of the fin in each case is constant at 13.1 cm^2 . The salient results of the analysis are listed in Table 5. Design 1 has six peripheral large holes as required to insert the MH lumps and sensor probes and 42 small holes. This fin configuration is used for experimental analysis. Designs 2, 3 and 4 with decreasing number of holes are analyzed and compared with design 1. It is found that more number of holes improve the performance and reduce the charging time. After 1000 s of absorption the average temperature of the fin is 325.7 K for design 2 whereas it is 329.0 K for design 4. The shortest absorption time for 10 g (1 wt%) of hydrogen is found as 560 s for design 2.

Effect of the hydrogen supply pressure

Effect of different supply pressure on absorption characteristics of MH has been studied at cooling fluid temperature of 298 K and flow velocity of 1 m/s. The MH bed temperature distribution in x-y plane at 68 mm from the top flange along the reactor height (in mid of two copper fins) is demonstrated at time $t = 120$ s, 720 s and 1200 s in Fig. 12(c) for different supply pressure of (a) 7 bar, (b) 11 bar and (c) 15 bar. High supply pressure of hydrogen increases the driving potential for mass transfer, which results in rapid absorption rate along

with enormous heat liberation. It is clear that the reaction is faster at high supply pressure; thus bed temperature approaches to predetermined cooling fluid temperature more rapidly as compared with low supply pressure. For example, at time $t = 1200$ s average bed temperature is around 305 K for 15 bar whereas it is more significant around 329 K in case of 7 bar.

The average bed concentration and average bed temperature are shown in Fig. 12(a) and (b) respectively. It is found that increase in supply pressure of hydrogen increases the absorption rate and thus reduces the charging time. It can be seen from Fig. 12(a) that for a supply pressure of 15 bar it takes 610 s to absorb 1 wt% of the hydrogen, which is 1080 s in case of 7 bar. Increase in reactor temperature is proportional to supply pressure as can be seen from Fig. 12(b). For a supply pressure of 15 bar, maximum bed temperature is found to be 356 K, which is just 333 K in case of 7 bar. High supply pressure decreases the time required for saturation and cools down the reactor much earlier as compared to low supply pressure.

Effect of cooling fluid temperature and velocity

Fig. 13(a) depicts the effect of cooling fluid temperature on the average bed concentration and average bed temperature. It is found that low temperature of the cooling fluid reduces the

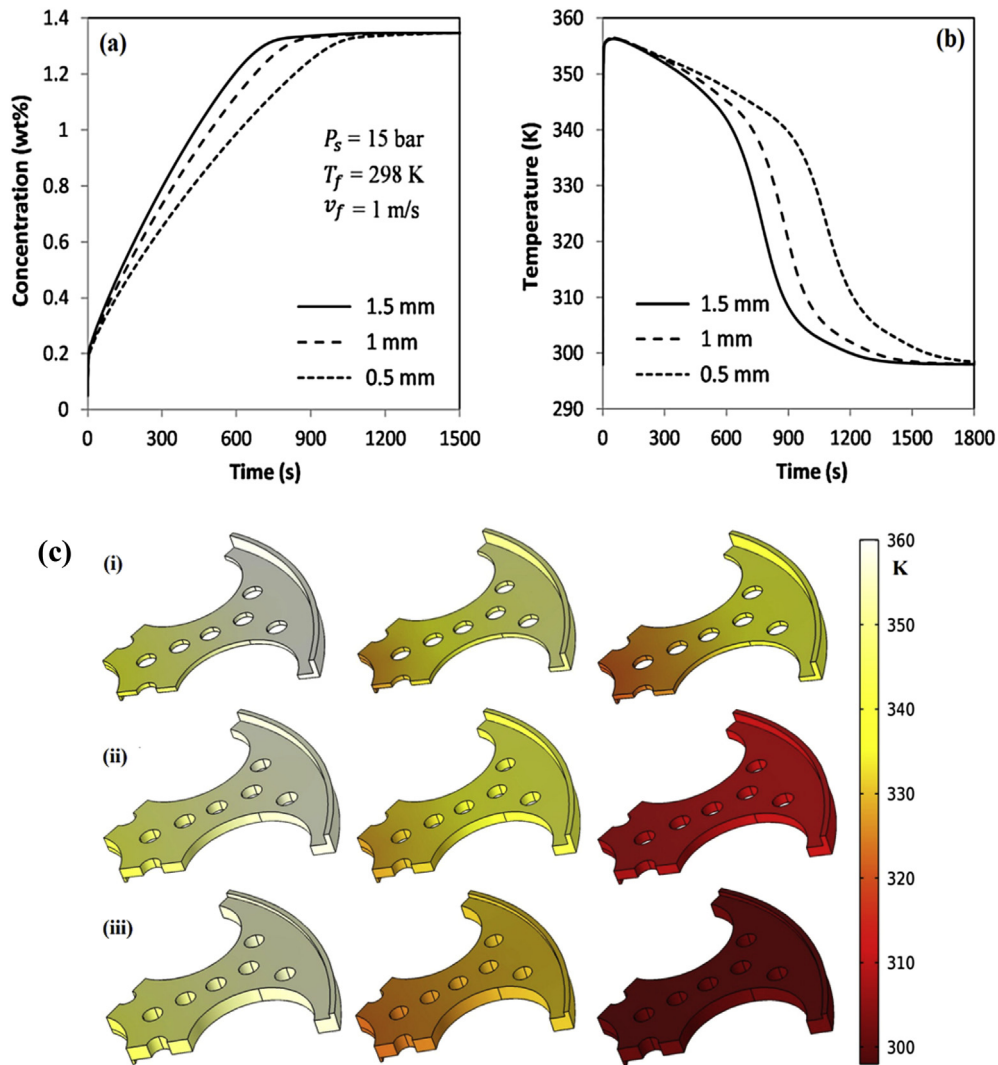


Fig. 10 – Effect of fin thickness on (a) average bed concentration and (b) average bed temperature and (c) temperature evolution in copper fin at $t = 120, 720$ and 1000 s, for (i) 0.5 mm, (ii) 1 mm and (iii) 1.5 mm.

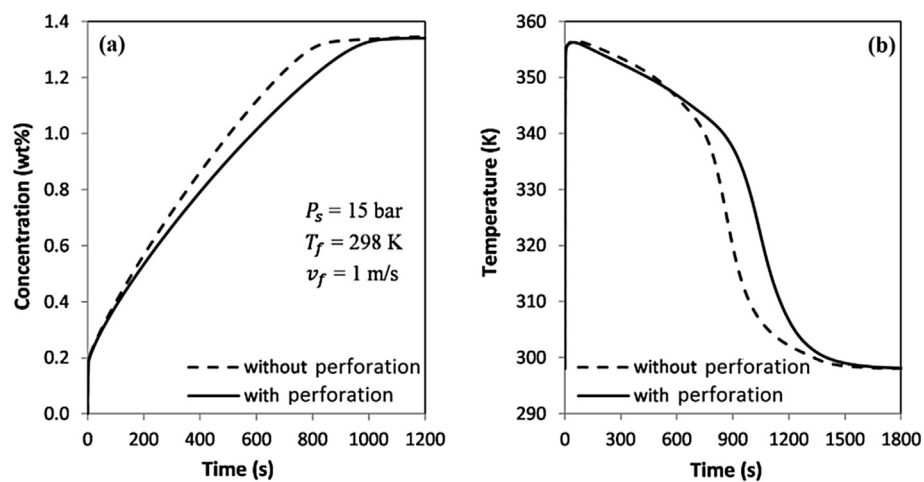
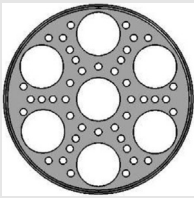
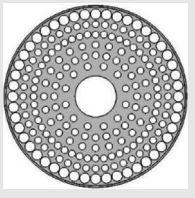
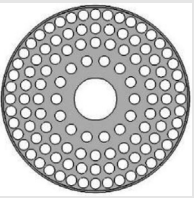
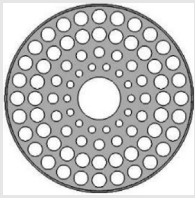

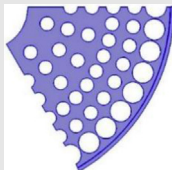
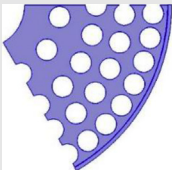

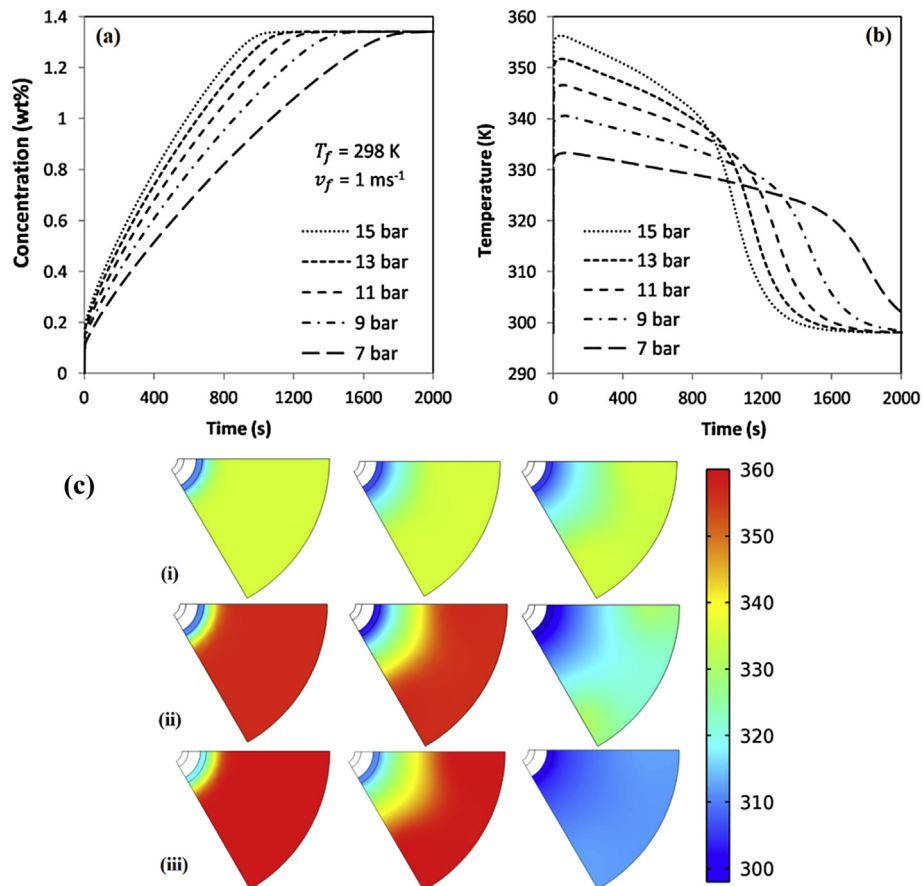


Fig. 11 – Effects of perforation in copper fin on (a) average bed concentration and (b) average bed temperature.

Table 5 – Effect of holes in copper fin on the performance of storage device

Design no.	Design 1 (actual design)	Design 2	Design 3	Design 4
Fin Design with different number of holes				
1/6th part of fin used for simulation analysis				
No. of holes	48	258	114	65
Surface area of fin	13.1 cm ²	13.1 cm ²	13.1 cm ²	13.1 cm ²
Charging time, s (for 10 g of H ₂)	614 s	560 s	582 s	604 s
Average temperature (K) of fin after 1000 s	330.2 K	325.7 K	326.5 K	329.0 K

**Fig. 12 – Effect of hydrogen supply pressure on (a) average bed concentration, (b) average bed temperature and (c) evolution of MH bed temperature in x-y plane at time $t = 120, 720$ and 1200 s for (i) 7 bar, (ii) 11 bar, (iii) 15 bar.**

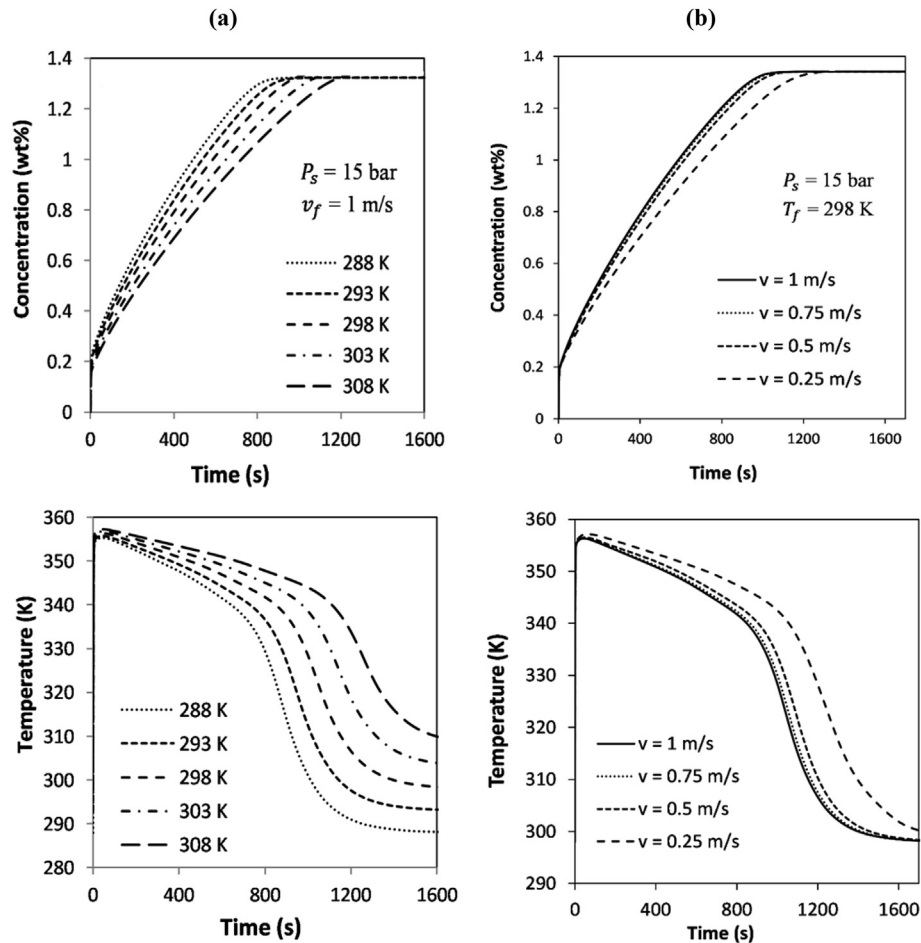


Fig. 13 – Effect of cooling fluid (a) temperature and (b) velocity on average bed concentration and average bed temperature.

charging time. Refer back to Fig. 5, in the first stage A, low temperature cooling fluid reduces the equilibrium pressure inside the reactor and thus increases the mass driving potential, which results in rapid absorption rate. Secondly in stage B, high temperature difference between the MH bed and cooling fluid enhances the heat transfer rate, which results in less charging time. It takes very less time to absorb the same amount of hydrogen at lower fluid temperature. It can be seen from Fig. 13(a) that for a cold fluid temperature of 288 K, it takes only 560 s to absorb 1 wt% of the hydrogen, which is found to be 760 s for cold fluid inlet of 308 K. Average bed temperature at time $t = 1200$ s is almost equal to 290 K for cooling fluid temperature of 288 K whereas it is found to be much higher 334 K in case of 308 K fluid temperature.

Fig. 13(b) depicts the effect of cooling fluid velocity on the average bed concentration and temperature. It is found that increase in velocity reduces the charging time. However, the improvement is not much significant beyond 0.75 m/s. Refer back to Fig. 5, cooling fluid velocity does not have any impact during stage A, because it only depends upon the supply pressure and equilibrium pressure of MH bed. But in stage B, since high velocity of cooling fluid increases the turbulence of the fluid, it enhances the heat transfer rate. Thus a higher value of cooling fluid flow velocity reduces the charging time.

It can be seen that at time $t = 1200$ s, bed temperature is found to be 322 K for cooling fluid velocity of 0.25 m/s whereas it is only 307 K in case of 1 m/s.

Conclusions

A novel design of solid state hydrogen storage device incorporating an inner heat exchanger tube with radial circular copper fins is proposed. A prototype is fabricated and experiments are performed with 1 kg LaNi₅ alloy. Simulation of the sorption phenomena in the storage device is carried out using COMSOL Multiphysics 4.4 software. The measured and predicted results are compared and a good agreement is obtained. Charging time of 18 min is obtained for supply pressure of 15 bar and cooling fluid temperature of 298 K and velocity of 1 m/s. Effects of different fin configurations and operating variables on absorption characteristics is investigated. Effects of supply pressure and cooling fluid temperature on bed performance is predominant. It can be concluded from the analysis that temporal variations in concentration and temperature are governed by pressure and temperature of operation. Due to small heat conduction path between the fins, transfer of heat is efficient and saturation is attained faster.

Increase in number and thickness of the fin enhances the absorption rate and reduces the charging time. However, the reactors developed by Linder et al. [13] and Anbarasu et al. [14] showed faster reaction kinetics than the present work. They have used a different MH ($\text{LaNi}_{4.91}\text{Sn}_{0.91}$) for the study and performed experiments at very high charging pressure whereas, LaNi_5 is used as a hydriding material for the present study and charging pressure is limited to 15 bar. Further, due to under performance of the present reactor, the reactor design has been upgraded with double tube heat exchanger which is under experimental study now.

Acknowledgment

This work is supported from the grants received from the Department of Science and Technology, Govt. of India towards the Project number DST/TSG/SH/2011/106-G.

Nomenclature

A	van't Hoff constant
B	van't Hoff constant, K
C	material constant, s^{-1}
c	hydride bed concentration, mol m^{-3}
c_p	specific heat, $\text{J kg}^{-1} \text{K}^{-1}$
D	diffusivity, $\text{m}^2 \text{s}^{-1}$
E	activation energy, J mol^{-1}
h	heat transfer coefficient, $\text{W m}^2 \text{K}^{-1}$
H_a	activation enthalpy, J
k	thermal conductivity, $\text{W m}^{-1} \text{K}^{-1}$
k_B	Boltzmann constant, J K^{-1}
\dot{m}	Volumetric mass flux of hydrogen, $\text{kg m}^{-3} \text{s}^{-1}$
MH	metal hydride
\vec{n}	normal vector
P	pressure, Pa
R	universal gas constant, $\text{J mol}^{-1} \text{K}^{-1}$
t	time, s
T	temperature, K
v	velocity, m s^{-1}
x	reacted fraction

Subscripts

a	absorption
d	desorption
e	effective
eq	equilibrium
f	fluid
g	gas
mh	metal hydride
s	supply
sat	saturation
0	initial

Greek letters

ΔH	heat of formation, J kg^{-1}
α	plateau slope
β	hysteresis factor
ϵ	porosity
ρ	density, kg m^{-3}

REFERENCES

- [1] Ben Nasrallah S, Jemni A. Heat and mass transfer models in metal in metal-hydrogen reactor. *Int J Hydrogen Energy* 1997;22:67–76.
- [2] Ram Gopal M, Srinivasa Murthy S. Prediction of heat and mass transfer in annular cylindrical metal hydrogen beds. *Int J Hydrogen Energy* 1992;17:795–805.
- [3] Ram Gopal M, Srinivasa Murthy S. Studies on heat and mass transfer in metal hydride beds. *Int J Hydrogen Energy* 1995;20:911–7.
- [4] Mohan G, Prakash Maiya M, Srinivas Murthy S. Performance simulation of metal hydride hydrogen storage device with embedded filters and heat exchanger tubes. *Int J Hydrogen Energy* 2007;32:4978–87.
- [5] Mellouli S, Askri F, Dhaou H, Jemni A, Ben Nasrallah S. A novel design of a heat exchanger for a metal-hydrogen reactor. *Int J Hydrogen Energy* 2007;32:3501–7.
- [6] Muthukumar P, Madhavakrishna U, Dewan Anupam. Parametric studies on a metal hydride based hydrogen storage device. *Int J Hydrogen Energy* 2007;32:4988–97.
- [7] Mellouli S, Dhaou H, Askri F, Jemni A, Ben Nasrallah S. Hydrogen storage in metal hydride tanks equipped with metal foam heat exchanger. *Int J Hydrogen Energy* 2009;34:9393–401.
- [8] Askri F, Ben Salah M, Jemni A, Ben Nasrallah S. Optimization of hydrogen storage in metal-hydride tanks. *Int J Hydrogen Energy* 2009;34:897–905.
- [9] Mellouli S, Askri F, Dhaou H, Jemni A, Ben Nasrallah S. Numerical simulation of heat and mass transfer in metal hydride hydrogen storage tanks for fuel cell vehicles. *Int J Hydrogen Energy* 2010;35:1693–705.
- [10] Anbarasu S, Muthukumar P, Mishra Subhash C. Test on $\text{LaNi}_{4.91}\text{Sn}_{0.15}$ based solid state hydrogen storage device with embedded cooling tubes – part A: absorption process. *Int J Hydrogen Energy* 2014;39:3342–51.
- [11] Souahlia A, Dhaou H, Askri F, Mellouli S, Jemni A, Ben Nasrallah S. Experimental study and characterization of metal hydride containers. *Int J Hydrogen Energy* 2011;36:4952–7.
- [12] Raju Mandhapati, Kumar Sudarshan. Optimization of heat exchanger design in metal hydride based hydrogen storage systems. *Int J Hydrogen Energy* 2012;37:2767–78.
- [13] Linder Marc, Mertz Rainer, Laurien Eckart. Experimental analysis of fast metal hydride reaction bed dynamics. *Int J Hydrogen Energy* 2010;35:8755–61.
- [14] Anbarasu S, Muthukumar P, Mishra Subhash C. Thermal modeling of $\text{LaNi}_{4.91}\text{Sn}_{0.15}$ based solid state hydrogen storage device with embedded cooling tubes. *Int J Hydrogen Energy* 2014;39:15549–62.
- [15] Wang Hui, Prasad Ajay K, Suresh Advani G. Hydrogen storage system based on hydride material with enhanced thermal conductivity. *Int J Hydrog Energy* 2012;37:290–8.
- [16] Chung CA, Yang Su-Wen, Yang Chien-Yuh, Hsu Che-Weu, Chiu Pai-Yuh. Experimental study on the hydrogen charge and discharge rates on metal hydride tanks using heat pipes to enhance heat transfer. *Appl Energy* 2013;103:581–7.
- [17] Muthukumar P, Singhal A, Bansal GK. Thermal modelling and performance analysis of industrial scale metal hydride hydrogen storage container. *Int J Hydrogen Energy* 2012;37:14351–64.
- [18] Ma Jincheng, Wang Yuqi, Shi Shaofei, Yang Fusheng, Bao Zewei, Zhang Zaoxiao. Optimization of heat transfer device and analysis of heat and mass transfer on the finned

- multi-tubular metal hydride tank. *Int J Hydrogen Energy* 2014;39:13583–95.
- [19] Souahlia A, Dhaou H, Mellouli S, Askri F, Jemni A, Ben Nasrallah S. Experimental study of metal hydride-based hydrogen storage tank at constant supply pressure. *Int J Hydrogen Energy* 2014;39:7365–72.
- [20] Mazzucco Andrea, Dornheim Martin, Sloth Michael, Jensen Torben R, Jensen Jens Oluf, Rokni Masoud. Bed geometries, fueling strategies and optimization of heat exchanger designs in metal hydride storage systems for automotive applications: a review. *Int J Hydrogen Energy* 2014;39:17054–74.
- [21] Mayer U, Groll M, Supper W. Heat and mass transfer in metal hydride reaction beds: experimental and theoretical results. *J Less-Common Metals* 1987;131:235–44.
- [22] Yang Fusheng, Cao Xinxin, Zhang Zaoxiao, Bao Zewei, Wu Zheu, Serge Nyallang Nyamsi. Assessment on long term performance of a LaNi_5 based hydrogen storage system. *Energy Procedia* 2012;29:720–30.